SAND--82-0542C

DE82 011027

A Ballistic Similitude Design Criterion for Artillery Projectiles

by

Albert E. Hodapp, Jr.* and Robert A. LaFarge*
Sandia National Laboratories, Albuquerque, N. M. 87185

---

*Member of Technical Staff, Division 5631, Aeroballistics (Member AIAA)

Abstract

A Sandia National Laboratorires analytically derived and experimentally verified Ballistic Simulitude Design Criterion (BSDC) is described herein. This BSDC, for projectiles of identical external shape, was used to guide development of the M753 8-inch Artillery Fired Atomic Projectile (AFAP) as a ballistically similar counterpart to the M650 8-inch rocket assisted conventional high explosive (HE) projectile. As required for simulitude, the mean impact point of the M753 falls within the precision error region about the M650 mean impact point when the M753 is fired with standard equipment and M650 firing data. The M753 is the first AFAP that has been developed and proven to be ballistically similar to a conventional HE projectile. Since gross internal differences between the M753 and M650 make complete duplication of M650 mass properties impossible, a BSDC was required to identify which properties were necessary to match in order to achieve simulitude. The effects of internal vibrating bodies, rotating band characteristics, muzzle exit conditions, the basic mass properties, and the effects of mass asymmetries were all considered in the development of this BSDC.

Introduction

Among the Military Characteristic (MC) requirements for the M753 rocket assisted (RA) 8-inch Artillery Fired Atomic Projectile (AFAP) was the requirement that it be ballistically similar to the M650 RA conventional high explosive (HE) 8-inch projectile. To satisfy the ballistic similitude requirement, the range and deflection differences between the mean points of impact for the M650 base projectile and the M753 AFAP must be respectively within one base projectile range and deflection probable error when the M753 is fired with M650 equipment and procedures at elevation and azimuth angles that differ with those of the M650 only by small differences that are determined by the allowable corrections. The corrections for the M753, defined by a U.S. Army ballistic similitude criterion, were determined from data obtained during a ballistic similitude verification test conducted at Yuma Proving Ground, Arizona during the fall of 1979. This ballistic similitude demonstration was a particularly significant event because the M753 is the first AFAP that has been developed and proven to be ballistically similar to a conventional projectile.

The subject matter of this paper is a description of the Sandia National Laboratories (SNL) analytically derived and experimentally verified Ballistic Similitude Design Criterion (BSDC) that was used to guide development of the M753 AFAP as a ballistically similar counterpart to the M650 conventional HE projectile. One obvious method to insure that an AFAP is ballistically similar to a rigid conventional projectile is to match the shape then adjust the mass properties of the AFAP to match those of the conventional projectile. Unfortunately the large differences in internal configuration that exist between an AFAP and a conventional projectile of identical external shape

may make it impossible to adjust all AFAP mass properties to match. Therefore a BSDC is required to define which critical properties must be matched in order to achieve similitude. Our BSDC is applicable to projectiles that have identical external shape like the M753 and M650 (Figure 1).

Projectile Motion Requirements and Analysis

To achieve ballistic similitude the dynamic behavior of the two projectile types must be closely matched. In this section we will discuss ballistic similitude requirements and projectile dynamics to provide a background for the derivation of our BSDC.

Trajectory

An artillery projectile is an aerodynamically unstable body that is stabilized by spinning about its axis of symmetry. Its spin rate is determined by the muzzle velocity and the twist of the rifling in the gun tube. As shown in Figure 2 for positive spin (clockwise as seen from the rear) the gyroscopic reaction to gravity induced trajectory curvature causes the projectile nose to rotate above (α_R) and to the right (β_R) of the velocity vector (flight path direction). The nose right component of this "yaw of repose" angle produces the aerodynamic force that cuases the projectile to drift to the right of its launch azimuth* (bore sight line). As shown in Figure 3, the projectile trajectory therefore has a crossrange component (deflection) in addition to its downrange component (range). The deflection which increases with increasing quadrant elevation (QE) angle**, can vary from a few tenths of one percent to about ten percent of the range. Therefore deflection as well as range is an important consideration for ballistic similitude.

---

*Azimuth angle increases in a clockwise direction from zero where the gun points due North.

**The angle between the gun tube centerline and a local horizontal is designated quadrant elevation (QE) because it is established with a Gunners quadrant (inclinometer).

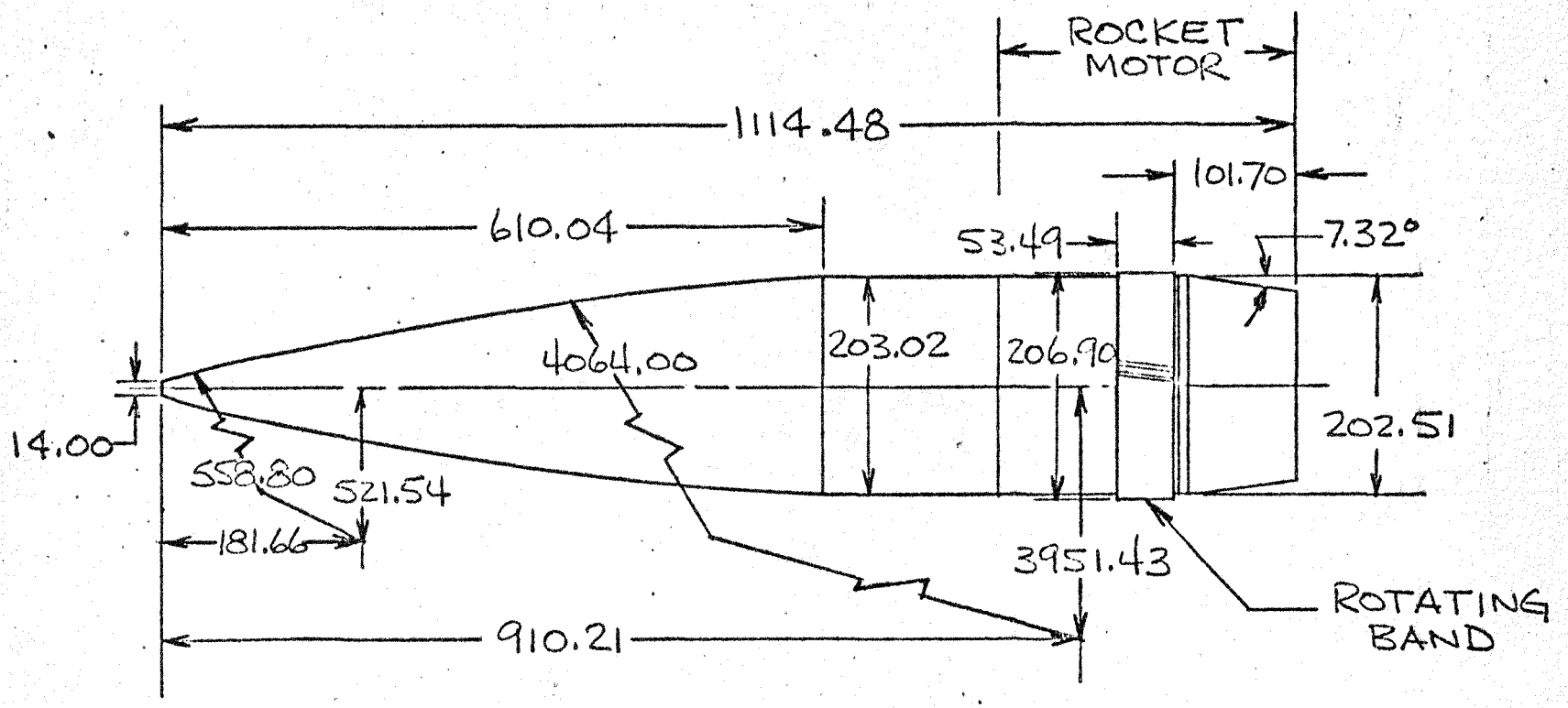

NOTE: ALL DIMENSIONS IN MILLIMETERS

Figure 1 External Dimensions of M650 and M753

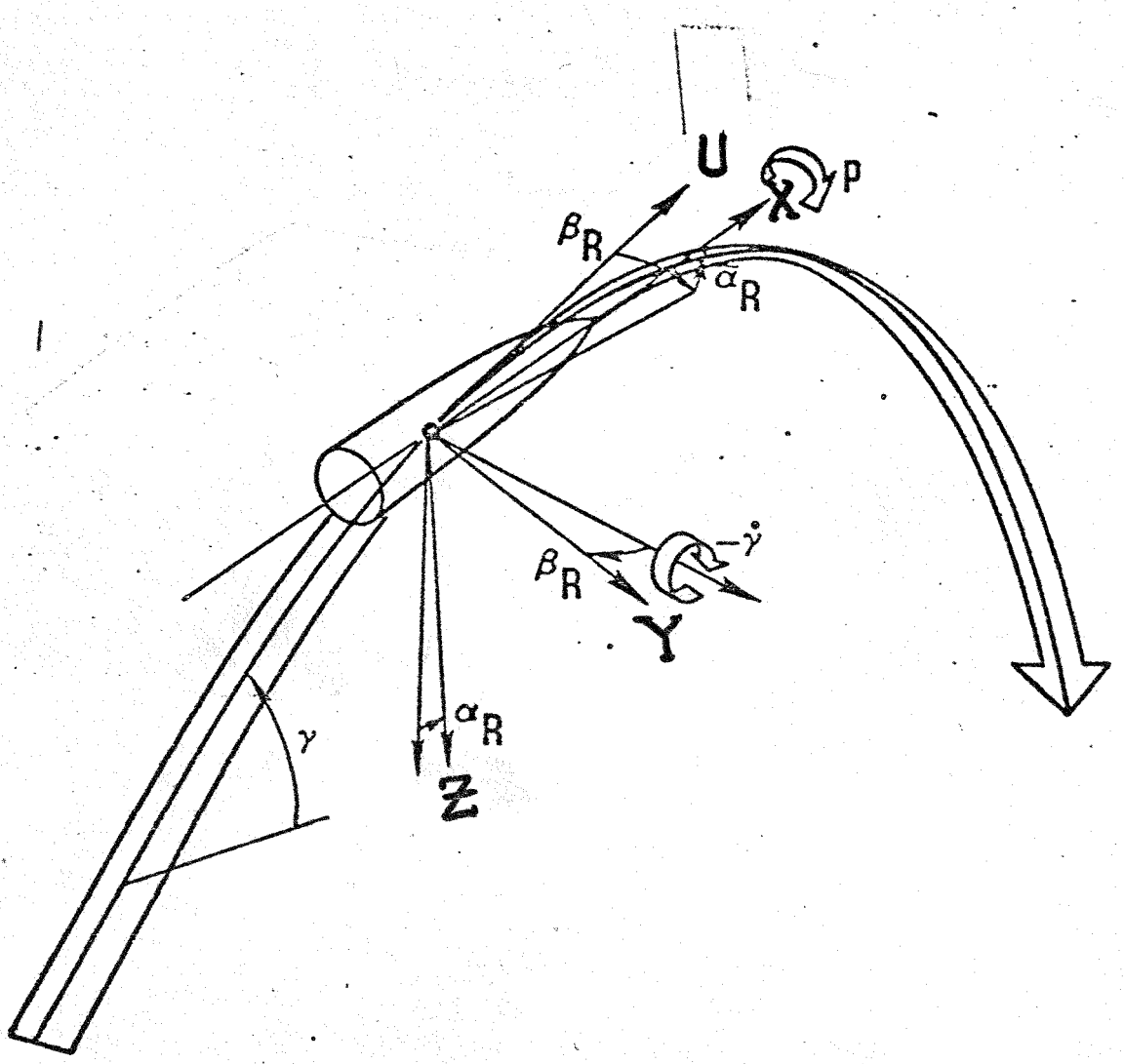

Figure 2 Yaw of Repose

	Range, m	RPE, m	Deflection, m	DPE, m
Maximum	30,000	76	2,400	15
Minimum	3,000	9	14	2

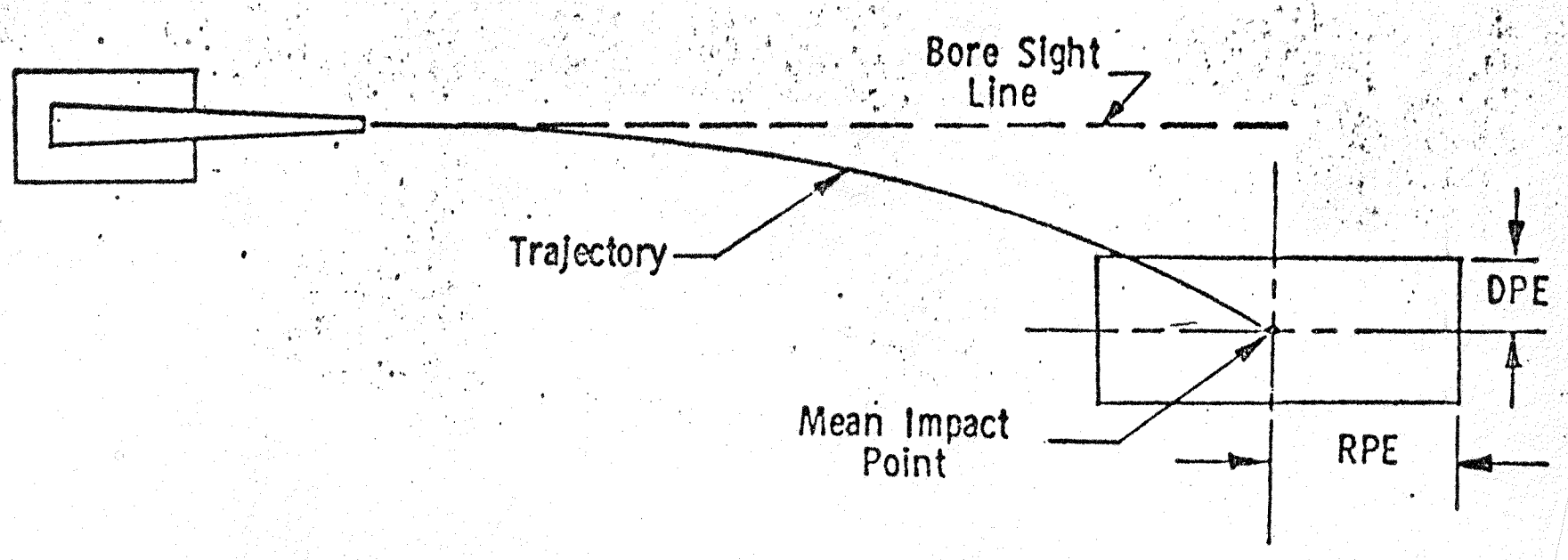

Figure 3 Trajectory Precision Error Specifications

Fig 3

Firing tables for a particular projectile and gun include range, deflection, range probable error (RPE), and deflection probable error (DPE) as a function of propelling charge type/zone and QE angle. As shown in Figure 3 the RPE and DPE form a rectangular "precision error region" about the mean impact point of the conventional base projectile. Small random variations in propelling charge performance, projectile physical characteristics, launch disturbances, etc., are all factors which effect the size of the RPE and DPE.

An AFAP meets Army ballistic similitude requirements with a conventional base projectile if its mean point of impact falls within the "precision error region" about the conventional projectile mean impact point (Figure 3) when the projectiles are fired at conditions which can differ only by the small differences in QE and azimuth angles determined by application of the allowable corrections. The small RPE and DPE values listed on Figure 3 for maximum and minimum values of range and deflection give an indication of how restrictive the ballistic similitude requirement actually is. Small corrections like the ones allowed are routinely used by artillerymen to account for variations in cannon performance and variations in lot-to-lot projectile and propellant characteristics. To apply the available corrections successfully, an AFAP must be closely matched to its conventional base projectile.

Projectile Dynamics

The dynamic model that we have chosen to represent the AFAP with is shown in Figure 4. All of the mass asymmetries that are known to effect dynamic behavior[1] can be included in this general model. A general model of a spinning projectile should include internal vibrating bodies because conditions exist where they are known to cause undesirable dynamic effects. Murphy[2] has shown that internal bodies should be rigidly attached to

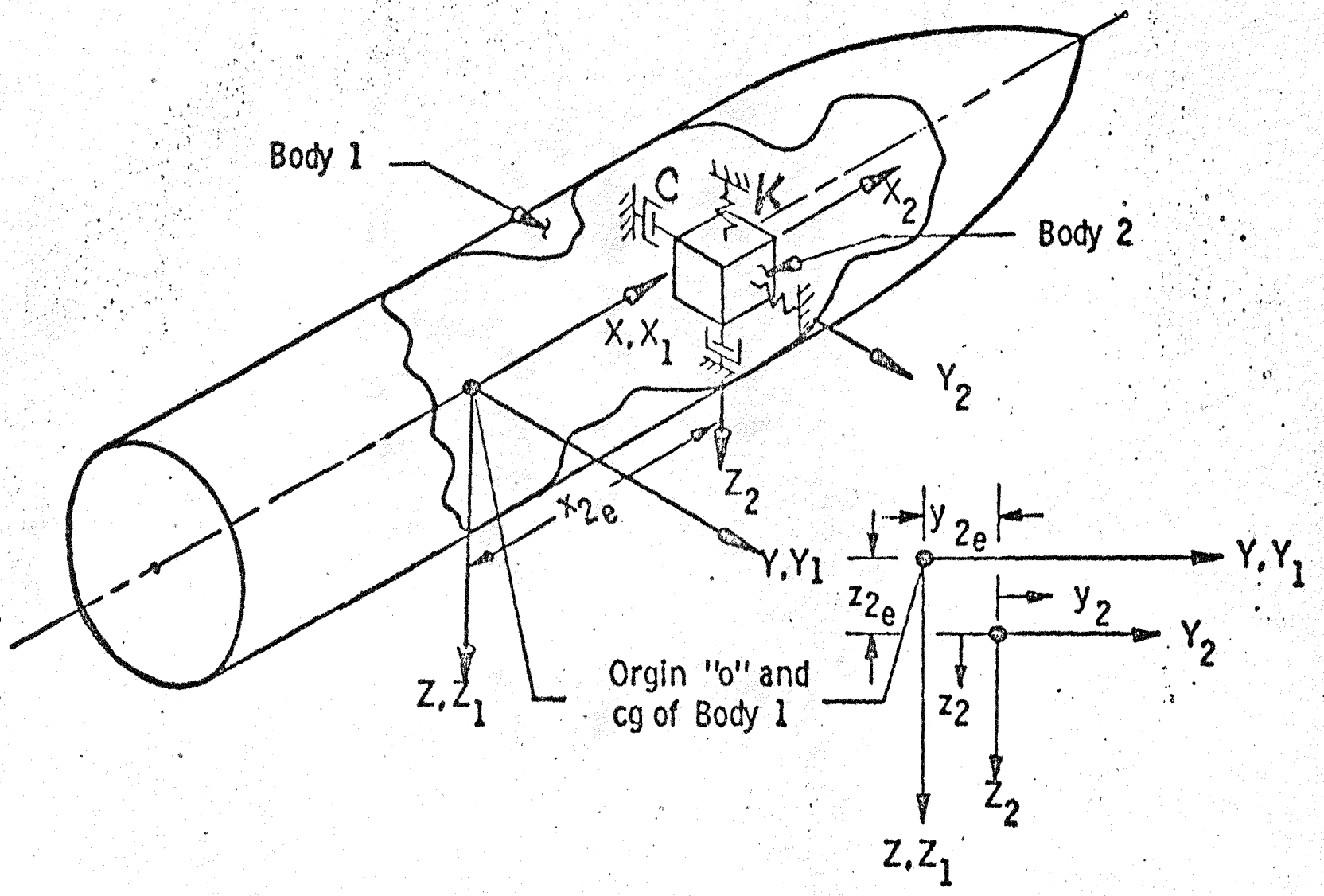

Figure 4 Projectile Dynamic Model

Fig 4

eliminate the possibility of serious flight instability. Our model is designed to provide information on the stability of rigidly attached vibrating internal bodies and their effects on projectile flight characteristics. For simplicity our model includes only one internal vibrating body. One is sufficient for demonstration purposes.

The two body system considered herein consists of an outer rigid (Body[1], Figure 4) that has a smaller rigid body (Body 2) suspended within it by two perpendicular massless springs. Viscous damping, C, is included in the model to simulate the presence of structural damping. Motion of Body 2 is constrained to translation in a plane parallel to the Y_1Z_1-plane; i.e., it can only move laterally. This model can represent cantilevered systems in bending as well as spring-mass systems in translation. Spring stiffness, K, is adjusted to give the internal vibrating body a critical frequency, p_{cr}, equal to the fundamental (lowest) vibration frequency of the system it simulates. For most cases of interest this provides an adequate dynamic model because the modal frequencies for the axial, torsional, and remaining bending modes are usually above the band of interest.

Motion of Body 1 is unrestrained. The $X_1Y_1Z_1$ body fixed axes (Body 1, Figure 4) and the XYZ reference axis system are coincident with their origins fixed on the centerline of Body 1 at "o". These coordinate systems and the $X_2Y_2Z_2$ system remain mutually parallel; therefore, both bodies have identical angular velocity. The $X_2Y_2Z_2$ system, located by the distances x_{2e}, $y_{2e}+y_2$, $z_{2e}+z_2$ from "o" along the respective axes, has its origin fixed at the cg of Body 2 (Figure 4). The cg of Body 1 is located by the vector $\bar{\rho}_{1cg}$ in the Y_1Z_1-plane; $\bar{\rho}_{1cg} = (0, y_{1cg}, z_{1cg})$.

The equations of motion for the two body system shown in Figure 4 are given relative to the XYZ body-fixed reference coordinates in Ref. 3. These equations were programmed into SANDSHELL[4] to provide trajectory

simulation results to study the motion of this eight-degree-of-freedom (8-DOF) two body system. To obtain more detailed information on the damping rates and modal frequencies that characterize the projectiles lateral motions, the differential equations of motion were linearized, reduced to eighth order, and solved numerically to obtain the eigenvalues and eigenvectors for the two body system. The motion patterns and regions of stability given by these results and those indicated by the complete 8-DOF simulations are in agreement.

The combined eigenvalue and eigenvector results indicate that when the critical frequency is greater than the roll rate ($p_{cr}>p$) the classical solution for the motion of a spinning rigid projectile, Eq. (2), can be used to describe the motion of a projectile with an internal vibrating body, while motion of the inner body can be adequately defined by Eq. (1) which neglects effects of projectile lateral angular motion. This is illustrated in Figure 5 by the excellent agreement between the numerically obtained eigenvalue components, represented by the circular symbols, and the analytically obtained values from Eqs. (1) and (2), represented by the solid lines. The condition $p_{cr}>p$ is imposed because motion of the inner body must be stable (λ_3 and $\lambda_4<o$) for projectile angular motion to be like that of an otherwise ballistically similar rigid body.

Our XYZ body-fixed reference coordinate system (Figure 4) is converted into a non-rolling-fixed-plane reference system like that used for Eq. (2)[5] by allowing the projectile to spin about the X-axis while the Y-axis moves in a plane that remains parallel to the earth tangent plane of an earth fixed inertial reference system. Angular orientation of the XYZ nonrolling

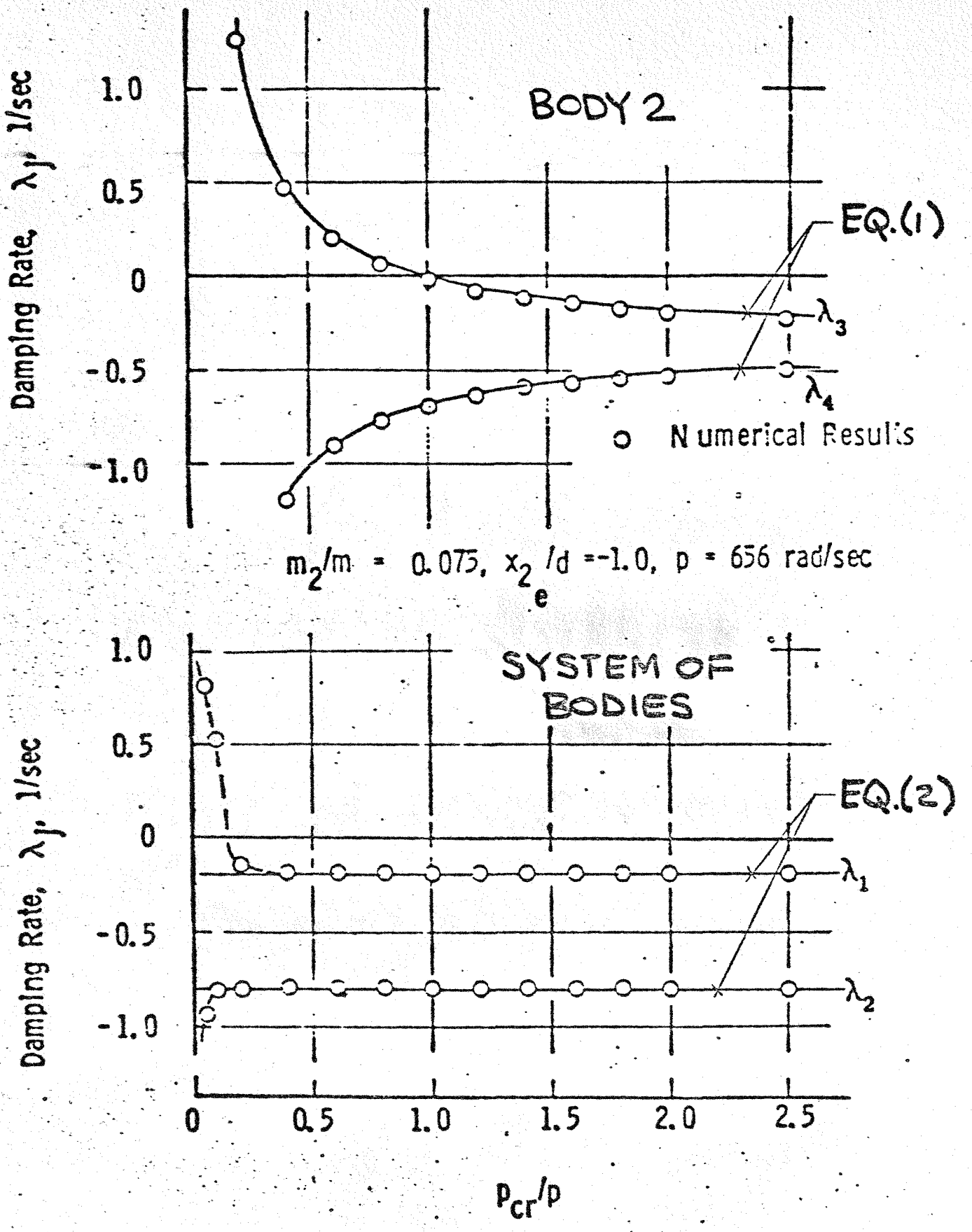

a. Damping Rates

Figure 5 Two Body System Eigenvalues

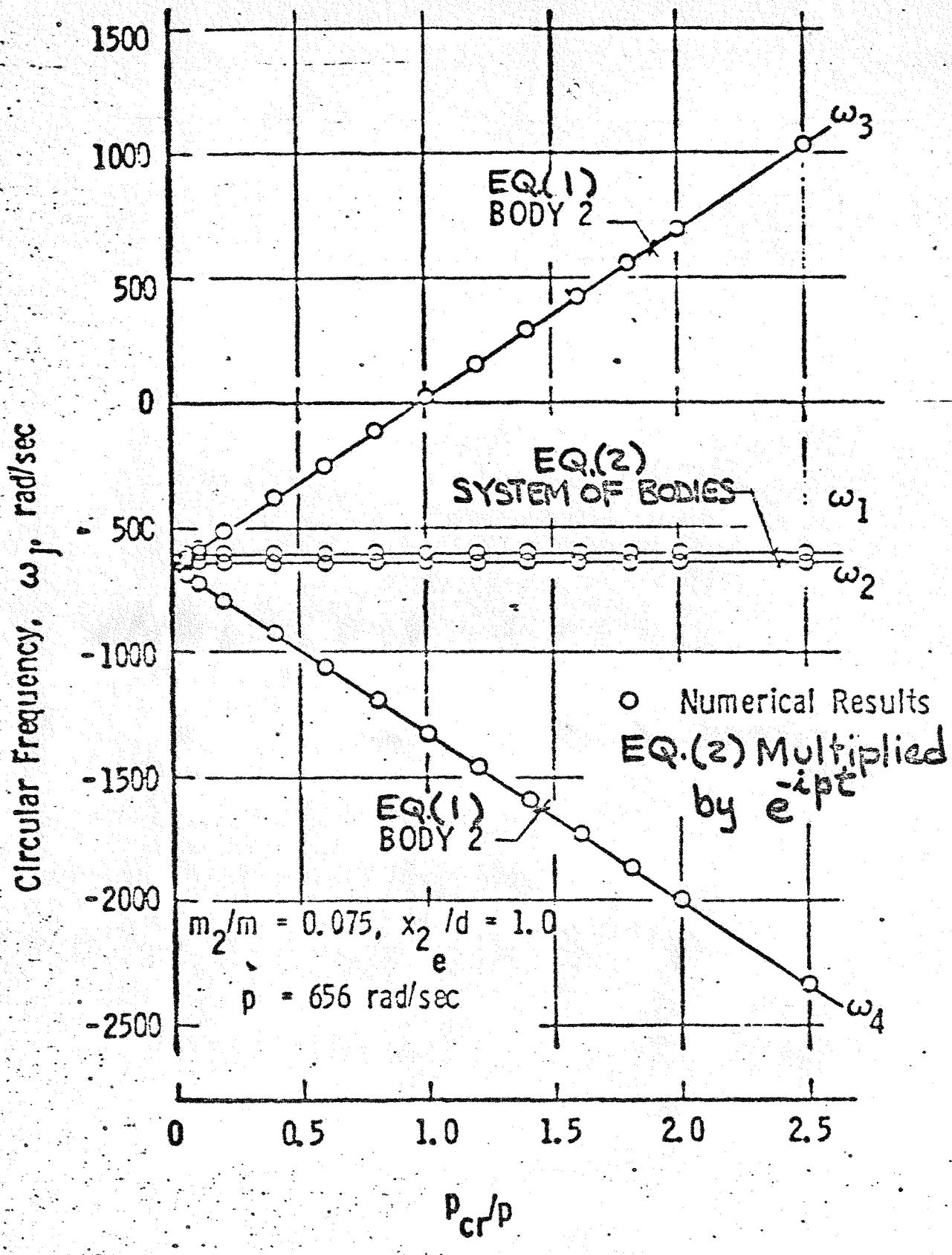

b. Circular Frequencies

Figure 5 (Concluded) Two Body System Eigenvalues

axes used for Eq. (2) is established relative to the earth fixed system by a yaw (ψ)-pitch (θ) sequence of Euler rotations. The position of the body-fixed Y_1 and Z_1 axes relative to the respective nonrolling Y and Z axes would then be given by the angle $\phi \approx pt$. When the XYZ reference axes are treated as body fixed, as they are for the results given in Figure 5, ϕ becomes the final Euler rotation in the ψ,θ,ϕ sequence. As indicated in Figure 5, Eq. (2) can be converted into a solution relative to the XYZ body-fixed reference axes of Figure 4 simply by multiplying through by e^{-ipt}.

Internal Body Motion. Assuming that the roll rate p remains constant, and neglecting the effects of the projectiles lateral angular motion, the motion of Body 2 (Figure 4) can be described as

$$\zeta = y_2 + iz_2 = D_3 e^{(\lambda_3 + i\omega_3)t} + D_4 e^{(\lambda_4 + i\omega_4)t} + D_5 \qquad (1)$$

where

$$\lambda_{3,4} = -\left(\frac{\eta}{2}\right)\sqrt{A}\ \left(p_{cr}\sqrt{A} \mp p\right)$$

$$\eta = C/C_c,\ C_c = \frac{m_1 m_2 p_{cr}}{m}, \qquad m = m_1 + m_2$$

$$p_{cr} = \sqrt{\frac{mK}{m_1 m_2}}$$

$$A = 1 + \frac{x_{2e}^2}{I}\left(\frac{m_1 m_2}{m}\right)$$

$$\omega_{3,4} = \pm\,(p_{cr}\sqrt{A} \mp p)$$

$$D_{3,4} = \frac{\mp i\dot{\zeta}_o + (p_{cr}\sqrt{A} \pm p)(\zeta_o - D_5)}{2p_{cr}\sqrt{A}}$$

$$D_5 = \zeta_e p^2/(p_{cr}^2\sqrt{A} - p^2)$$

$$\zeta_e = y_{2e} + iz_{2e}$$

The complex total lateral displacement of Body 2, ζ, given by Eq. (1), is composed of damped lateral displacement components, D_3 and D_4 with circular frequencies ω_3 and ω_4, and a steady component, D_5, which results from asymmetrical placement of Body 2 within Body 1 (y_{2e} and/or $z_{2e} \neq 0$, Figure 4). Equation (1) indicates that transient lateral motions of Body 2 are stable (λ_3 and $\lambda_4 < 0$) only when $p_{cr} > p/\sqrt{A}$. At $p_{cr} = p/\sqrt{A}$ a resonance occurs causing D_5 to become unbounded. The 8-DOF trajectory simulation results show the same behavior with p_{cr}/p, except at resonance where diverging lateral displacement is accompanied by an unpredicted rapid decrease in roll rate. To avoid the possibility of unstable internal body motion

and resonance induced structural failure, the critical frequency of Body 2 motion must be greater than the highest attainable value of $p/\sqrt{A}$. Flight data obtained to support the work presented in Ref. 6 has established that Eq. (1) provides an accurate model of internal body motion for $p_{cr} > p/\sqrt{A}$.

System Angular Motion. With the exception of the requirement to eliminate effects of internal body motion $p_{cr} > p/\sqrt{A}$, our BSDC is derived from the classical solution for the motion of a spinning rigid projectile which is given as.

$$\tilde{\xi} = \tilde{\beta} + i\tilde{\alpha} = K_1 e^{(\lambda_1 + i\omega_1)t} + K_2 e^{(\lambda_2 + i\omega_2)t} + K_3 e^{ipt} + K_4 \qquad (2)$$

where

$$\lambda_{1,2} = \frac{1}{2}\left(\frac{q'S}{mU}\right)\left\{\left[\left(C_A - C_{N_\alpha}\right) + \left(\frac{md^2}{2I}\right)\left(C_{M_q} + C_{M_{\dot{\alpha}}}\right)\right]\left(1 \pm \tau\right) \mp 2\tau\left[\left(C_A - C_{N_\alpha}\right) - \left(\frac{md^2}{2I_X}\right)C_{M_{p\alpha}}\right]\right\}$$

$$\tau = 1/\sqrt{1 - 1/S_g}$$

$$S_g = \left(\frac{pI_X}{2I}\right)^2 \Big/ \left(\frac{q'SdC_{M_\alpha}}{I}\right)$$

$$C_{M_\alpha} = C_{N_\alpha}\left(X_{cg} - X_{cp}\right)/d$$

$$\omega_{1,2} = \left(\frac{pI_X}{2I}\right)\left[1 \pm 1/\tau\right]$$

$$K_{1,2} = -\tau \left\{\left[\left(\delta_\beta - \frac{\tilde{q}_o}{p}\right) + i\left(\delta_\alpha - \frac{\tilde{r}_o}{p}\right)\right]\left[\frac{I}{I_X} - \frac{1}{2}\left(1 \mp 1/\tau\right)\right] + \frac{p}{2U}\left(z_{cg} - iy_{cg}\right)\left(1 \mp 1/\tau\right)\right\}$$

$$K_3 \approx \left(\delta_\beta + \frac{pz_{cg}}{U}\right) + i\left(\delta_\alpha - \frac{py_{cg}}{U}\right)$$

$$\delta_\alpha \approx J_{XZ}/(I - I_X),\ \delta_\beta \approx J_{XY}/(I - I_X)$$

$$y_{cg} = \frac{1}{m}\left(m_1 y_{1cg} + m_2 y_{2e}\right),\ z_{cg} = \frac{1}{m}\left(m_1 z_{1cg} + m_2 z_{2e}\right)$$

$$m = m_1 + m_2$$

$$K_4 = \beta_R + i\alpha_R, \quad \beta_R \approx \frac{-pI_X\dot{\gamma}}{q'SdC_{M_\alpha}}$$

$$\dot{\gamma} = g\cos\theta/U$$

The complex total angle-of-attack, $\tilde{\xi}$, given by Eq. (2) and shown graphically in Figure 6 is composed of damped transient angular motion components, the nutation K_1 and precession K_2 vectors with circular frequencies ω_1 and ω_2, and steady components, the constant magnitude body-fixed trim vector K_3 with circular frequency p, and the quasi-steady fixed yaw of repose K_4. Equation (1) is a quasi-steady solution to linearized equations of projectile motion relative to a nonrolling fixed-plane reference coordinate system.[5] The form of this solution is most desirable for our purposes because it describes the projectile angular motion that is detected by an earth-fixed observer. It is applicable over consecutive or overlapping short time intervals of the

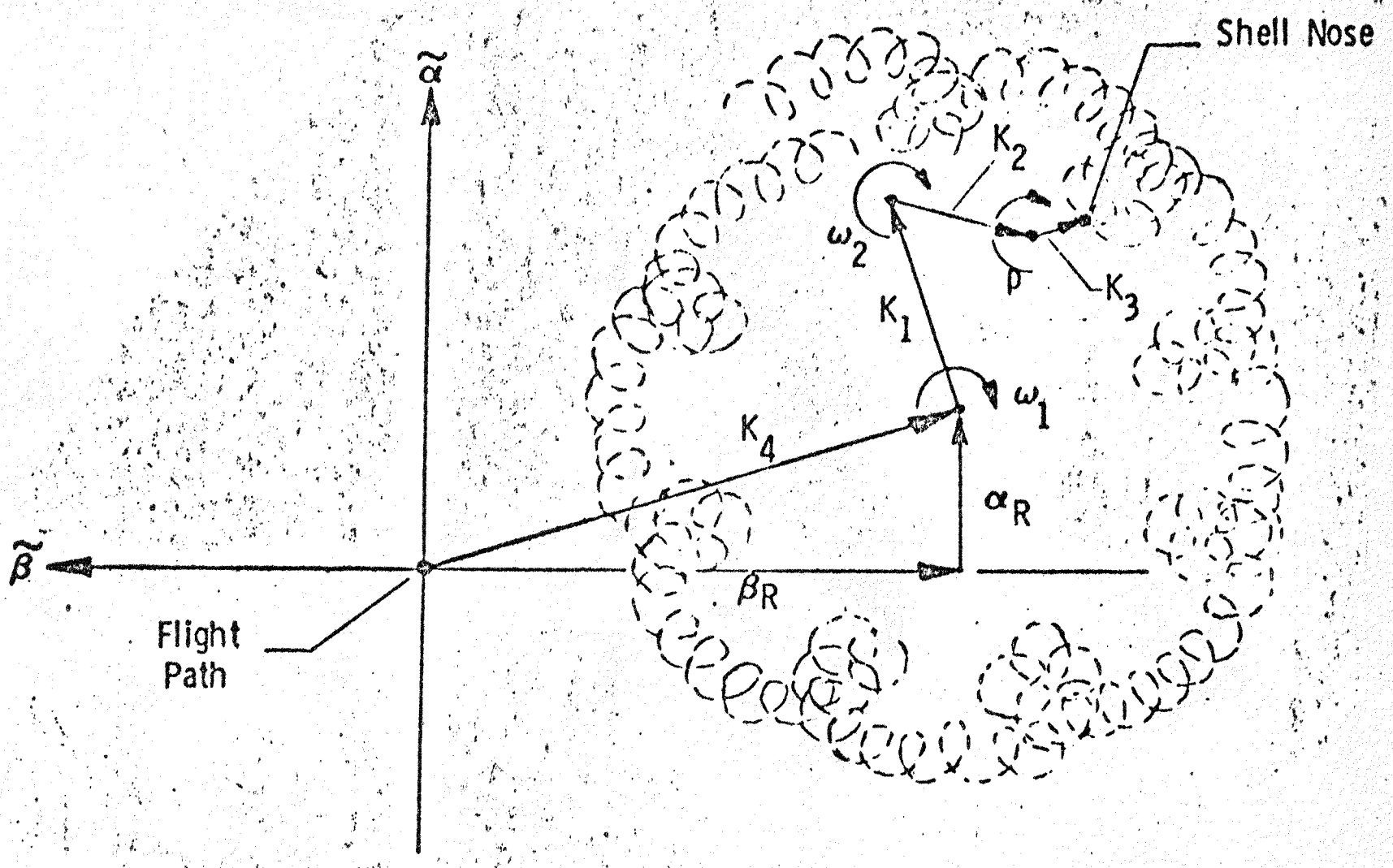

Figure 6 Complex Nonrolling Total Angle of Attack

Fig 6

projectile trajectory where the roll rate p, the dynamic pressure q', and trajectory elevation angle θ can be considered approximately constant.

As shown in Eq. (2), there are no resonance conditions for angular motions of the aerodynamically unstable ($C_{M_\alpha} > 0$) spin stabilized ($S_g \geq 1$) projectile. By requiring that $p_{cr} > p/\sqrt{A}$, we eliminate the possibility of a large contribution to projectile angular motion that could result from transient instabilities or resonances of inner body motion. The conditions for stable projectile angular motion indicated by Eq. (2) are λ_1 and $\lambda_2 < 0$ and $S_g \geq 1$. These are not absolute stability conditions because Eq. (2) does not account for the effects of changing dynamic pressure, q', on the convergence or divergence of the projectiles angular motion. However, when the above stability conditions are satisfied, the effects of changing dynamic pressure are usually small.

Throughout many firing zones of interest, particularly in the more important high muzzle velocity long range zones, the transient angular motion damps rapidly after muzzle exit so that only the trim angle $K_3 e^{ipt}$ and yaw of repose K_4 remain. Since the direct contribution of trim angle to angular motion is negligibly small and because $|\beta_R| >> |\alpha_R|$ for all except the highest QE firing conditions, the β_R component of the yaw of repose K_4, Eq. (2) can become the primary contribution to angular motion over a large portion of the flight. The β_R component is negligibly small near muzzle exit, reaches its maximum magnitude near mid trajectory, then reduces in magnitude as the projectile descends toward the ground. The maximum magnitude of β_R increases with increasing QE and can exceed fifteen degrees for the 8-inch projectiles and QE bands considered herein. As

indicated earlier in the discussion of Figure 2, the aerodynamic force produced by β_R is responsible for the large trajectory deflections. The drag induced by β_R can effect range. Therefore, β_R is obviously of primary interest for ballistic matching.

The effect on range of the damped transient angular motion cannot be ignored. Large differences in the damping rates λ_1 and λ_2 between projectiles and large differences in the initial magnitude of their transient angular motions can produce unacceptably large differences in range. Results presented in Eq. (2) indicate that the initial maximum of the damped transient angular motion, $|\tilde{\xi}|_{fm} \approx |K_1| + |K_2|$ (first maximum yaw), is determined by the projectile pitch and yaw rates at muzzle exit ($\tilde{q}_o$ and $\tilde{r}_o$) and by the projectile mass asymmetries (δ_α, δ_β, y_{cg}, and z_{cg}) that form the small trim angle $K_3 e^{ipt}$. Although the direct contribution of the trim angle to projectile angular motion is negligibly small, its principal axis misalignment components δ_α and δ_β can have a large effect on first maximum yaw $|\tilde{\xi}|_{fm}$ through their effect on the initial magnitude of K_1 and K_2, Eq. (2). The center-of-gravity offset contributions to K_3, y_{cg} and z_{cg}, have little effect on the magnitude of K_1 and K_2 except for critically low gyroscopic stability ($S_g \approx 1.0$), a condition that is avoided.

Similitude Requirements

The range of a spin stabilized projectile is determined by muzzle velocity U, QE, and effective ballistic coefficient $W/C_D S$. Ballistic coefficient is reduced, hence range is reduced, by the increased drag that results from projectile angular motion. For a given muzzle velocity,

deflection depends on projectile weight, W, and on the β_R component of the yaw of repose K_4. Our BSDC for projectiles having identical external shape requires rigid body characteristics and a match between muzzle velocity, ballistic coefficient, β_R, and mass asymmetry induced effects on transient angular motion. The quantities we have identified to match in order to satisfy these requirements are listed in Table I.

Muzzle Velocity

Small differences in muzzle velocity can have a large effect on range differences between projectiles. For projectiles having identical shape and weight, muzzle velocity can be matched by using the base projectile rotating band with an underlying structure that has response characteristics similar to that of the base projectile. It is important to have similar rotating band characteristics, otherwise differences in muzzle velocity between the base and matching projectiles can vary with gun wear level. This could defeat the ballistic similitude objective because there are no firing table corrections available to account for differences of this type. Problems of this type were avoided with the M753 and M650, because the rotating band is attached to the rocket motor assembly that is common to both projectiles.

Mass Property Effects

Since the projectiles have identical shape, they have the same reference area S. The drag coefficient C_D, which is approximately the same for both projectiles, is a function of shape, surface condition, and the magnitude of projectile angular motion. Basic assumptions used in formulating this

Table I, BSDC Requirements for Projectiles of Identical External Shape

Characteristics to be Matched	Quantities to Match	Effects
Rigid Body	$p_{cr} > p/\sqrt{A}$	Range and Structural Integrity
Muzzle Velocity, U	W, Rotating Band Characteristics	Range
Ballistic Coefficient, $W/C_D S$	W	Range
Yaw of Repose, β_R	I_X, X_{cg}	Deflection
Mass Asymmetry Effects	$\delta\left\{1 + \left(\frac{2I}{I_X} - 1\right) \tau\right\}$	Range

Note: Substantial differences in lateral moment of inertia, I, can exist between projectiles when S_g is sufficiently large.

BSDC are that differences in the magnitude of the yaw of repose, differences in the magnitude of the transient angular motion about the yaw of repose (Figure 6), and differences in surface condition will all have at most a small but correctable effect on relative range and deflection. Therefore, in order to match ballistic coefficient, the weight W of both projectiles must be matched.

If projectiles with the same shape and weight are to have the same yaw of repose induced deflection, β_R must also be the same. Vaughn and Wilson[7] in their earlier work on ballistic similitude have shown that in order to match β_R between projectiles under these conditions, the ratio of the moment of inertia I_X about the projectile axis of symmetry (X-axis, Figure 4) to the distance along the X-axis between the center of gravity X_{cg} and the center of pressure X_{cp}, $I_X/(X_{cg}-X_{cp})$, must be the same for both projectiles. This is derived by equating the β_R expression given in Eq. (2) for two projectiles, then canceling p, $\dot{\gamma}$, q', S, and C_{N_α}, terms that would be equivalent for two ballistically similar projectiles. Because of identical Mach number induced variations of X_{cp} which occur when identical shapes are used, it may not be possible to achieve a sufficiently close match of the above ratio for a full range of flight Mach number conditions when the magnitudes of I_X and X_{cg} are appreciably different from those of the base projectile. Therefore, the most realistic approach to assure that deflection is matched for the general flight condition is to attempt to match I_X and X_{cg} individually.

None of the above restrictions effect the moment of inertia I about an axis through "o" (Figure 4) perpendicular to the X-axis of symmetry

($I = I_Y = I_Z$). Experience gained through evaluating 6-DOF trajectory simulation results and flight test results has indicated that for projectiles with sufficiently high minimum values of gyroscopic stability factor, like the M753 and M650, moderate differences in I between otherwise ballistically similar projectiles produce only small differences in the first maximum yaw $|\tilde{\xi}|_{fm}$ induced by $\tilde{q}_o$ and $\tilde{r}_o$ and small differences in the damping rates of the respective transient angular motions. These small differences in transient angular motion result in correctable differences in relative mean impact point. This is fortunate because W, I_X, and X_{cg}, as you will note later, are AFAP physical characteristics that can be closely matched to those of a conventional base projectile when the requirement for matching I can be relaxed.

A series of firing/flight tests were conducted at the SNL Tonopah Test Range (TTR) in Nevada to verify that portion of our BSDC concerned with the effects of I_X, I, and X_{cg}. Specially prepared M106 8-inch artillery projectiles were used for these experiments. Results taken from Ref. 8, are given in Figure 7. Each of the mass properties I, I_X, and X_{cg} were varied separately while the weight W and the remaining mass properties were held at fixed reference levels (R subscripts in Figure 7). Flight test results confirm the prediction that deflection is strongly effected by mismatches in I_X and X_{cg} but not effected by a mismatch in I. Furthermore, range was found to be insensitive to realistic variations in I, I_X, and X_{cg} in both the predictions and flight test results.

Mass Asymmetry Effects

The large random values of $\tilde{q}_o$ and $\tilde{r}_o$ that occur at the extremes of their probability distributions cause large magnitudes of first maximum yaw. Very small principal axis misalignment angles, like those that can

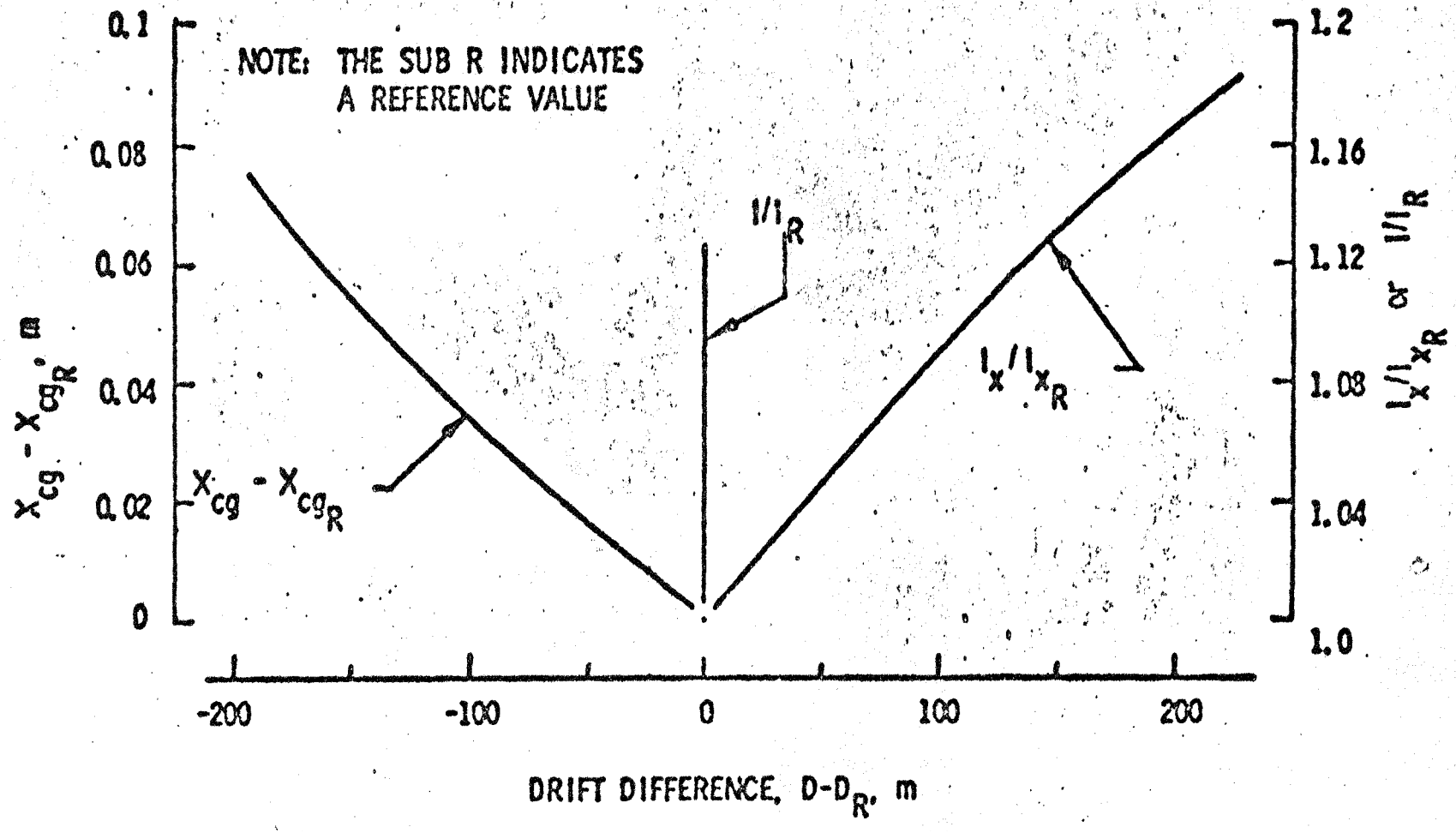

Figure 7 Yaw of Repose Test Results

Fig 7

exist within an AFAP, can produce initial disturbances larger than those produced by the extremes of $\tilde{q}_o$ and $\tilde{r}_o$. Small differences in principal axis misalignment can produce sufficiently large differences in transient angular motion to cause more than a correctable difference in range to occur[1,5] Therefore, matching or reducing the effects of principal axis misalignment is an important consideration for ballistic similitude.

A principal axis misalignment exists when the longitudinal principal axis of a projectile is angularly misaligned with the gun induced spin axis (ideally the projectile axis of symmetry). When the projectile exits the gun tube the principal axis becomes the natural spin axis. Overshoot in the alignment of the spin axis produces a disturbance in the projectiles transient angular motion that is very large in comparison with the principal axis misalignment angle. The maximum amplitude of this overshoot in the initial transient angular motion (first maximum yaw) is approximately $2I/I_X$ times the total principal axis misalignment angle $\delta = \sqrt{\delta_\alpha^2 + \delta_\beta^2}$ (Table I) except for gyroscopic stability factors S_g near one where the gain can become a factor of several hundred. As shown in Ref. 5, the damping that we have ignored for simplicity will prevent the first maximum yaw from becoming unbounded as $S_g \to 1$, $\tau \to \infty$.

In addition to investigations with analytical models and SANDSHELL[4], the dependence of first maximum yaw, hence range, on principal axis misalignment was investigated with a firing/flight test using specially prepared M106 8-inch projectiles and the gun used for the previous test[9]. These projectiles were ballistically matched except for differences in principal axis misalignment angle. The predictions and flight test results shown in Figure 8 demonstrate

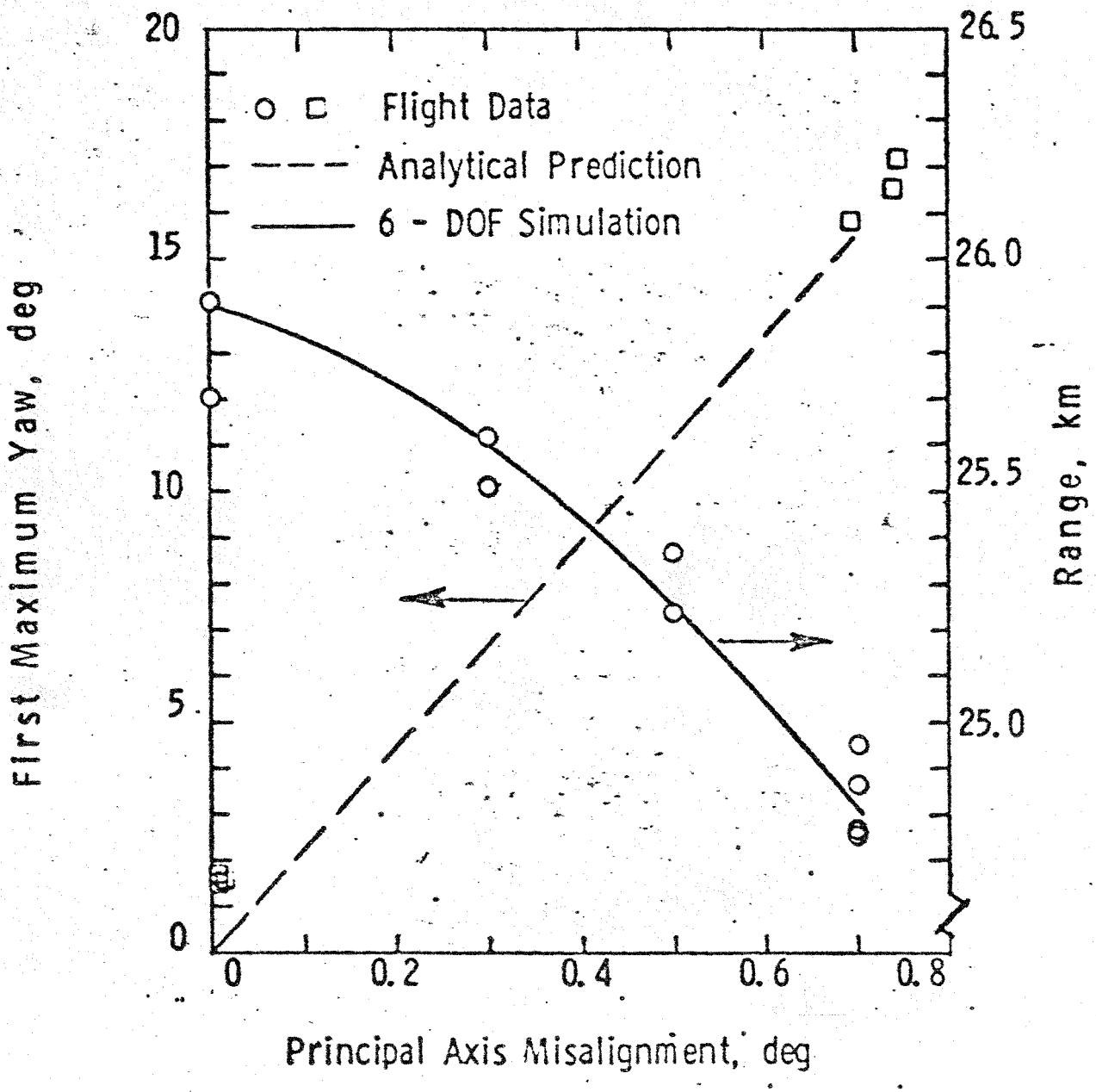

Figure 8 Principal Axis Misalignment Test Results

Fig 8

that small differences in principal axis misalignment can produce large variations in first maximum yaw and unacceptably large differences in range. Range reductions were particularly small for these tests because the high gyroscopic stability levels for these projectiles kept the first maximum yaw near its minimum value.

An AFAP will generally have a larger principal axis misalignment angle than a conventional HE projectile. Reducing AFAP principal axis misalignment to match the mass asymmetry induced first maximum yaw of the conventional base projectile is an important consideration for similitude (Table I). This is particularly true for high air density arctic sea level conditions with muzzle velocities slightly below the speed of sound because first maximum yaw can become very large under these minimum gyroscopic stability conditions.

Ballistic Similitude Demonstration

Measured mean values for the mass properties of fifty-five M753 and two hundred twenty M650 projectiles used for the ballistic similitude verification test are given in Table II along with the Fire Control Input (FCI) values which define the mean mass properties of the M650. Lateral moment of inertia, I, and principal axis misalignment angle, δ, are not used to build firing tables, therefore they are not listed with the FCI values. Although the M753 projectiles were fired with dummy nuclear systems, the mass properties of these projectiles are representative of those for the M753 AFAP.

To achieve ballistic similitude with the M650, the M753 was developed according to the SNL BSDC, Table I, so that its weight, W, center of

Table II, M753 and M650 Mass Properties

	M650 FCI Standard Values	M753 Test Projectiles	M650 Test Projectiles*
W, lb (kg)	200.0 (90.72)	200.0 (90.72)	198.9 (90.22)
X_{cg}, in(m)	29.28 (0.7437)	29.36 (0.7457)	29.22 (0.7422)
I_X, lb-in^2 (kg-m^2)	1911 (0.5592)	1903 (0.5569)	1917 (0.5610)
I, lb-in^2 (kg-m^2)	--	15983 (4.6773)	15543 (4.5486)
δ, deg	--	0.027	0.022

*Corrected to a 2.06 lb (0.934 kg) M557 fuze weight.

gravity location, X_{cg}, and axial moment of inertia, I_X, are all closely matched to those of the FCI standard M650. The M753 has rigid body characteristics. Its rotating band and support structure are those of the M650. The small differences in I_X and X_{cg}, indicated in Table II, and the larger difference in lateral moment of inertia, I, all resulted in correctable differences in relative mean impact point with the M650 throughout all firing zones. Principal axis misalignment for the M650, as shown in Table II, was far below the level that would noticeably effect range. For this case it was not necessary to reduce M753 principal axis misalignment to match M650 mass asymmetry induced effects. Instead M753 principal axis misalignment angle was reduced to a minimum practical value that would also have a negligible effect on range.

Examples of corrected range differences between the M753 AFAP and M650 are given as a function of QE in Figure 9 for three separate firing zones representative of minimum, medium, and maximum range applications. Dashed lines in Figure 9 are M650 RPE boundaries. Differences in mean impact points, solid lines, were determined by fitting a mathematical model (6-DOF simulation results) to the experimental data points (circular symbols). The results given in Figure 9 clearly demonstrate that the range differences between the M753 and M650 mean points of impact are less than one M650 RPE. Deflection differences, not shown, are less than one DPE. Therefore, results of the ballistic similitude verification test prove that the M753 is ballistically similar to the M650.

Conclusion

An analyticall derived and experimentally verified Ballistic Similitude Design Criterion (BSDC) was developed at Sandia National Laboratories (SNL)

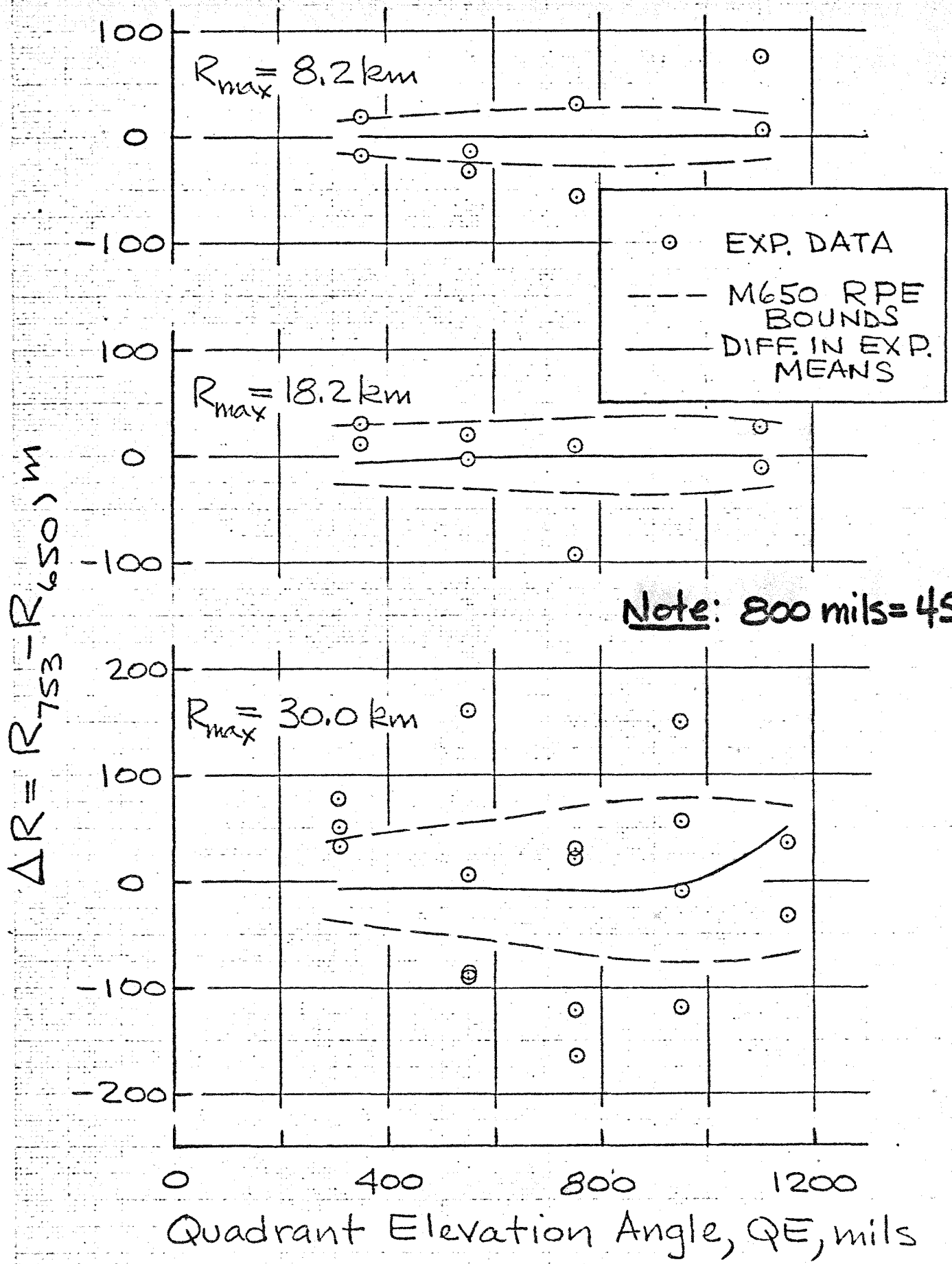

Figure 9 Ballistic Similitude Verification Test Results for M753

to provide a means for developing an Artillery Fired Atomic Projectile (AFAP) to be ballistically similar to a rigid conventional high explosive (HE) projectile of identical external shape. Gross differences in internal configuration between an AFAP and a conventional HE projectile often make it impossible to adjust all AFAP mass properties to match. Therefore, a BSDC is required to identify which critical properties must be matched in order to achieve similitude. The SNL BSDC for rigid projectiles of identical external shape requires that the rotating band characteristics, weight, center of gravity position, axial moment of inertia, and principal axis misalignment induced effects all equal those of the conventional base projectile. Lateral moment of inertia does not have to be matched to achieve similitude. This feature is responsible for the success of the SNL BSDC because the remaining AFAP mass properties can be closely matched to those of the conventional projectile when the requirement to match lateral moment of inertia is relaxed.

Our experience in evaluating this BSDC for several AFAP configurations, utilziing 6-DOF trajectory simulations, is that the resulting differences in range and deflection with the base projectile are sufficiently small to be easily corrected within the ballistic similitude requirements using the allowed corrections. The SNL BSDC was used to guide development of the M753 8-inch AFAP as a ballistically similar counterpart to the M650 8-inch rocket assisted conventional HE projectile. Results obtained from a ballistic similitude verification test for these projectiles prove that the M753 is ballistically similar to the M650. This event has twofold significance: first, because it proves the applicability of this BSDC

using real hardware; and second, because the M753 is the first AFAP that has been developed and proven to be ballistically similar to a conventional HE projectile.